CHAPTER **2**

Normal bones and joints

John Graham and Massimo Vignoli

KEY POINTS

❚ The mineral content of bone means it is ideally suited to radiographic assessment.
❚ Two orthogonal projections are the minimum requirement for assessing most bone structures.
❚ Incomplete mineralization in juvenile patients can obscure injury and make interpretation challenging.
❚ Radiographs of the contralateral limb or a control subject may help distinguish normal anatomic variation from pathology.
❚ Radiographic remodeling from injury may take 3 to 5 days to become evident in juvenile patients and over 10 days in mature patients.

Radiography of the skeleton

Bone is in many ways the ideal structure for assessment by radiographs, and the first radiographic image ever obtained was of a human hand. The mineral content of bone ensures good radiographic contrast with surrounding soft tissues and shows the internal structure. Survey radiographs are the first-line diagnostic choice to evaluate patients for skeletal disease, skeletal trauma, and skeletal manifestations of systemic disease. For most body parts, two orthogonal projections, such as mediolateral and craniocaudal radiographs, are the minimum requirement. Oblique images may be needed to assess complex joints such as the carpus and tarsus. Radiographs of long bones should include the joints at the proximal and distal extents (**fig. 2.1**). Radiographs of the joints should be centered on the joint itself and include the adjacent long bones (**figs. 2.2** and **2.3**). Unless there is a clinical contraindication, sedation or anesthesia are recommended for most patients to assist in obtaining consistent diagnostic positioning. Radiographs of the contralateral limb, a healthy sibling, or a normal age-matched cat or dog of the same breed can be very helpful in distinguishing pathology from normal variation in immature patients. It is important to remember that bone is a living, dynamic structure constantly undergoing remodeling by osteoblasts and osteoclasts. This is more obvious in juvenile patients when an insult to the bone may result in radiographically visible changes within 3 to 5 days. In mature patients, remodeling changes may take up to 10 to 14 days to become visible on radiographs. It is recommended that the reader acquire an atlas of normal radiographic anatomy to assist in interpretation.
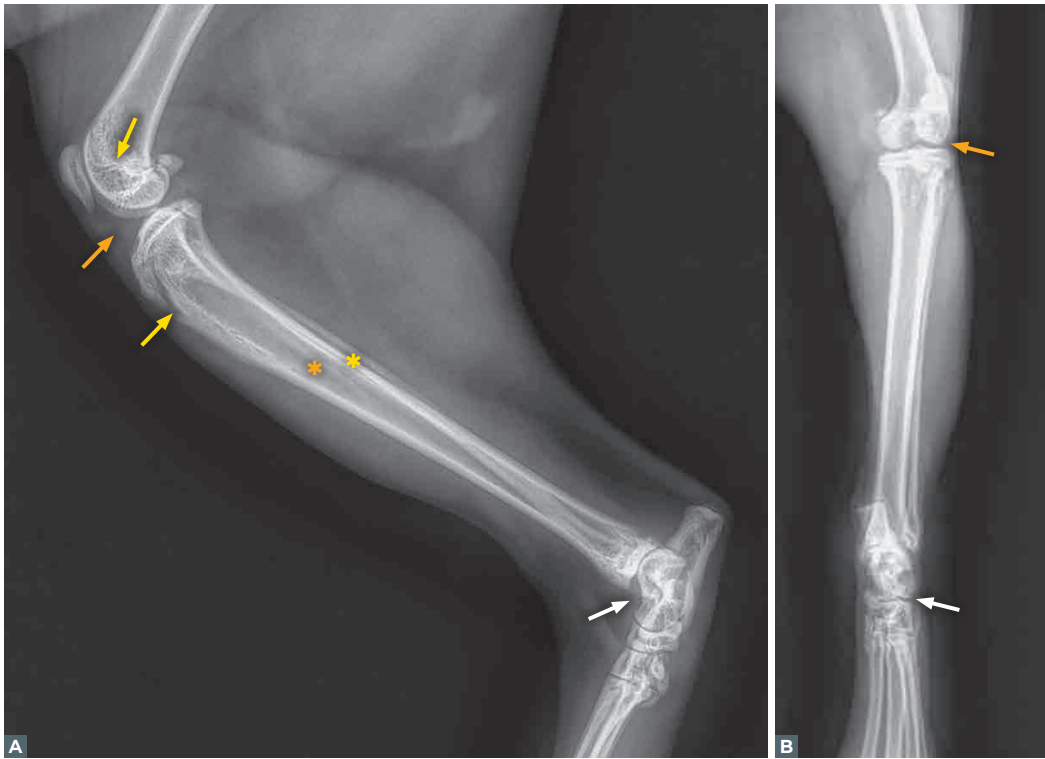
Fig. 2.1 Normal radiographic study of the right hind leg of a 14-month-old spayed female British shorthair cat. Radiographs of long bones should include the joints at the proximal and distal extents, in this case, the stifle (orange arrows) and tarsus (white arrows). The growth plates of the distal femur and the tibial tuberosity are incompletely closed (yellow arrows). The tibial (orange asterisk) and fibular (yellow asterisk) diaphyses are normal.
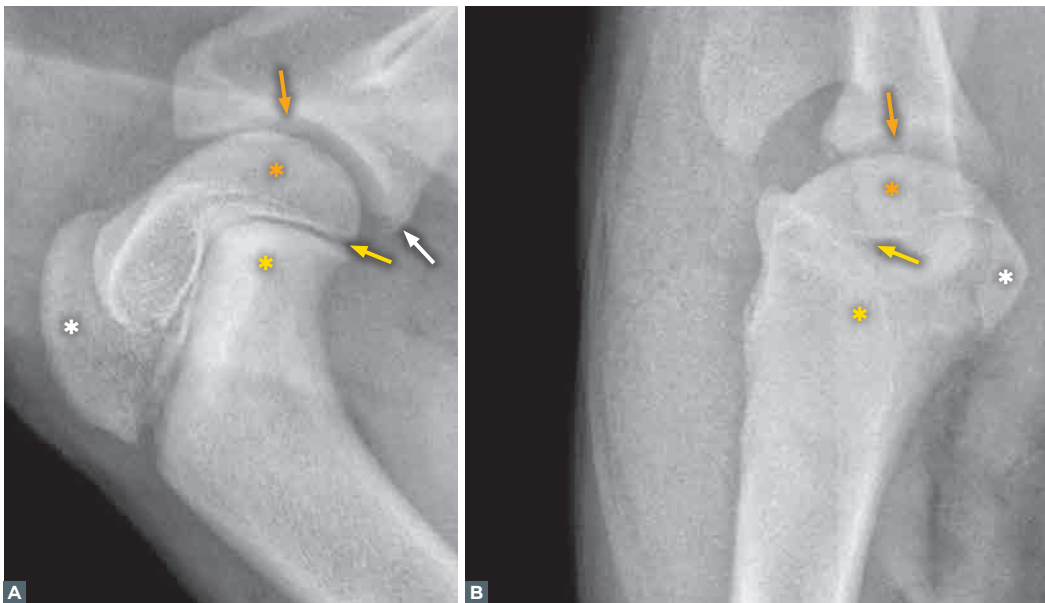

Fig. 2.2 Mediolateral and caudocranial projections of a normal shoulder of a five-month-old female mixed breed dog. Radiographs show the glenoid cavity (orange arrows), humeral head or proximal epiphysis (orange asterisks), physis (yellow arrows), and proximal metaphysis (yellow asterisks). There is incomplete ossification of the caudal margin of the glenoid (white arrow). The cranioproximal margin of the greater tubercle of the humerus is indistinct from incomplete ossification (white asterisks).

Ultrasound of the skeleton is used for the assessment of skeletal disease. Ultrasound is reflected at the bone surface and can assess bone margins for proliferation or lysis. Ultrasound is more helpful in the evaluation of the soft tissues of the musculoskeletal system, such as tendons, ligaments, muscles, joint capsules, and effusions or articular cartilage (**figs. 2.4** and **2.5**).

Fig. 2.3 Mediolateral radiograph of the humerus of a four-month-old Mastiff with a history of intermittent lameness. The radiograph is normal and shows features of a juvenile skeleton with incomplete mineralization. Open growth plates are visible in the proximal humerus, distal humerus, and proximal radius (arrows). There are separate ossification centers of the supraglenoid tubercle, medial epicondyle of the humerus, and olecranon (asterisks), separated from the adjacent bones by a radiolucent growth plate. The proximal humeral epiphysis is completely mineralized, but there is no visible mineralization of the greater tubercle of the proximal humerus.
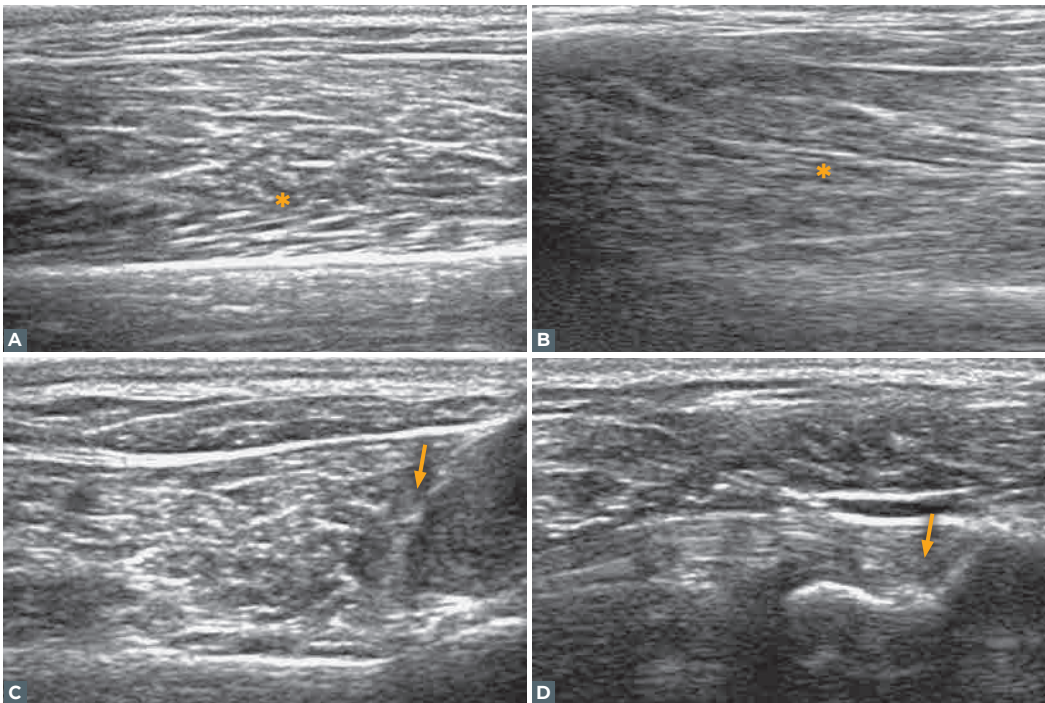

Fig. 2.4 A five-year-old spayed female mixed breed dog. The images show a normal supraspinatus muscle (asterisks) **(A)** and its tendon at the insertion on the greater tubercle (arrow) of the humerus **(B)**. The normal infraspinatus muscle **(C)** (asterisk) and its tendon **(D)** at the site of insertion on the greater tubercle (arrow), just distal to the most proximal point.

Fig. 2.5 Ultrasound of the shoulder joint of a dog. The image shows the biceps tendon of the origin (orange arrows) at the supraglenoid process of the scapula (asterisk). A small amount of fluid is visible deep in the tendon in the joint capsule and tendon sheath (white arrows).
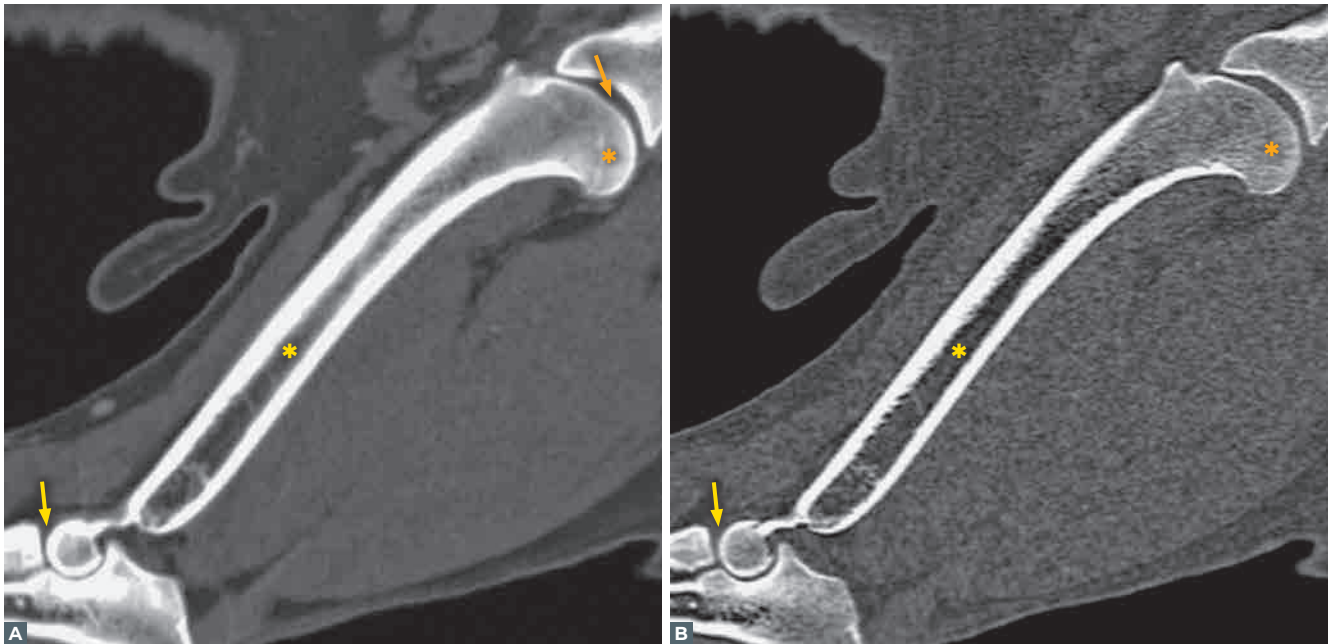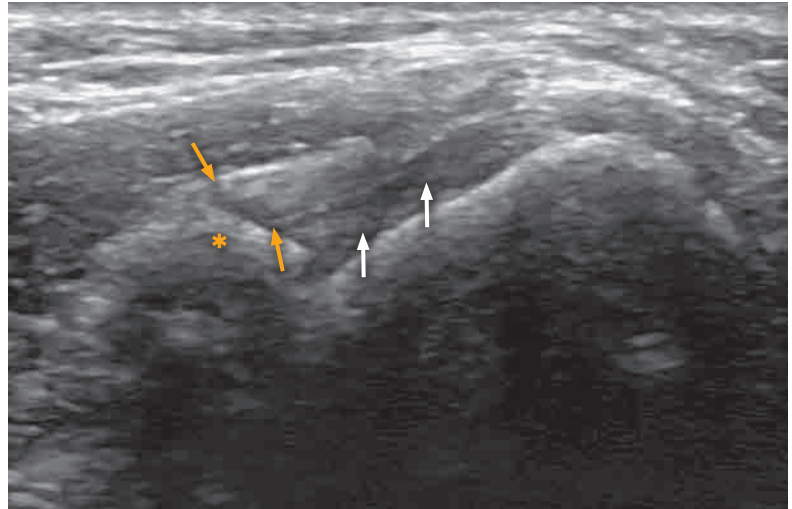

Fig. 2.6 Computed tomography sagittal plane reconstruction of a normal humerus in soft tissue window **(A)** and bone window **(B)** of a three-year-old spayed female Samoyed. Shoulder joint (orange arrows), elbow joints (yellow arrows), epiphyses (orange asterisks), and diaphyses (yellow asterisks) are shown. Note the honeycomb-like trabecular bone within the epiphyses and metaphyses.

Computed tomography (CT), as it uses X-rays, is superbly adapted to imaging bone, with superior contrast to radiographs and the capacity for detailed imaging of internal bone structure. Images acquired in thin slices can be reprocessed in multiplanar reconstructions (MPR) to highlight specific structures (**figs. 2.6-2.9**). MRI is slightly less suitable for imaging bone pathology, as it depends upon the water content of tissue, which is limited in normal bone. MRI is the imaging modality of choice for evaluating the soft tissue structures of the skeleton, particularly intra-articular structures, because of its excellent contrast resolution and capacity to acquire images in any plane (**fig. 2.10**).
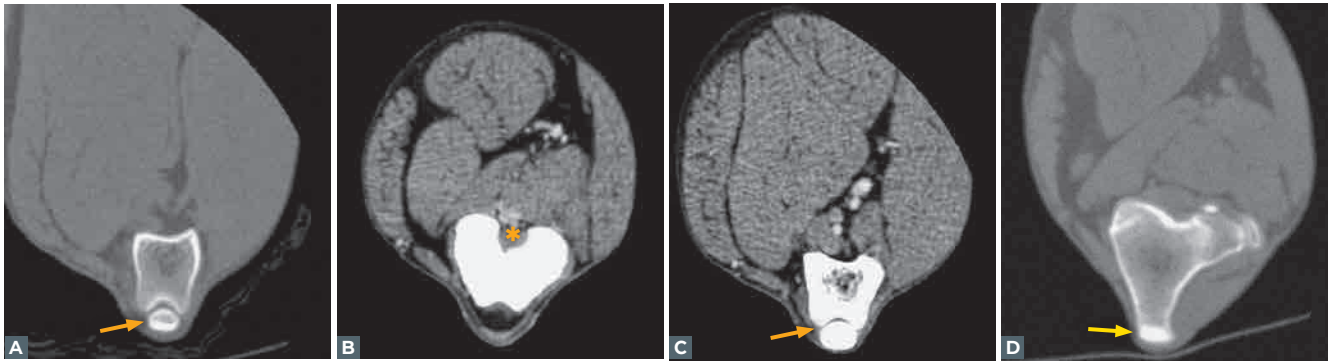
Fig. 2.7 Computed tomography images of a normal knee of an adult male Dobermann. Bone **(A)** and soft tissue **(B)** windows at the level of the femoral trochlea and patella (orange arrows). Distal to it **(C)**, the intercondyloid fossa with the origin of the cruciate ligaments (asterisk) is visible. **(D)** Shows the tibial crest, the insertion site of the patellar (quadriceps) tendon (yellow arrow).
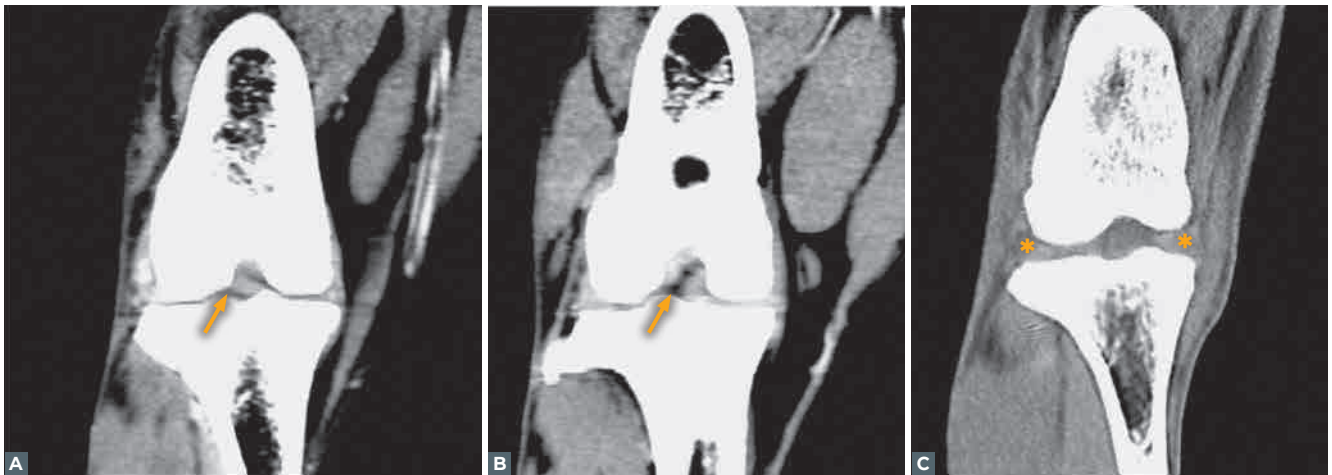
Fig. 2.8 Multiplanar dorsal reconstructions of the knee of the same dog as in fig. 2.7 in soft tissue window. Cranial **(A)** and caudal **(B)** cruciate ligaments are well visible (arrows), as well as the menisci **(C)** (asterisks).

Fig. 2.9 Same dog as in fig. 2.7 in a soft tissue window sagittal reconstruction. **(A)** The cranial cruciate (orange arrow) ligament, **(B)** the crossing (yellow arrow) of the ligaments, and **(C)** the caudal cruciate (white arrow) ligament are clearly visible.

Fig. 2.10 MRI of a normal stifle joint of a dog in sagittal T2 and 3D HYCE, and in dorsal high-resolution gradient echo. The patellar (quadriceps) tendon (orange arrows), infrapatellar fat (asterisks), cranial and caudal cruciate ligaments (yellow arrows),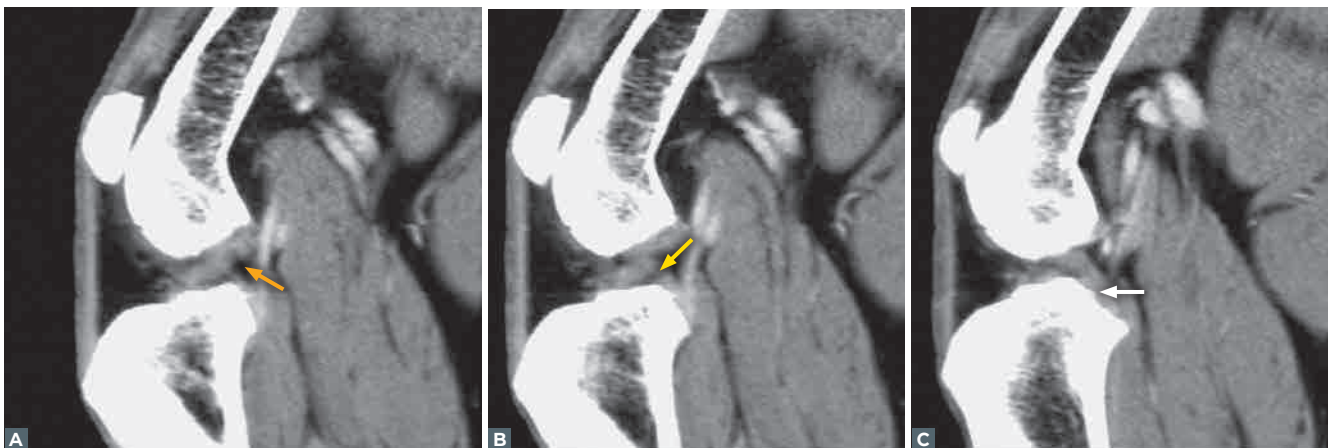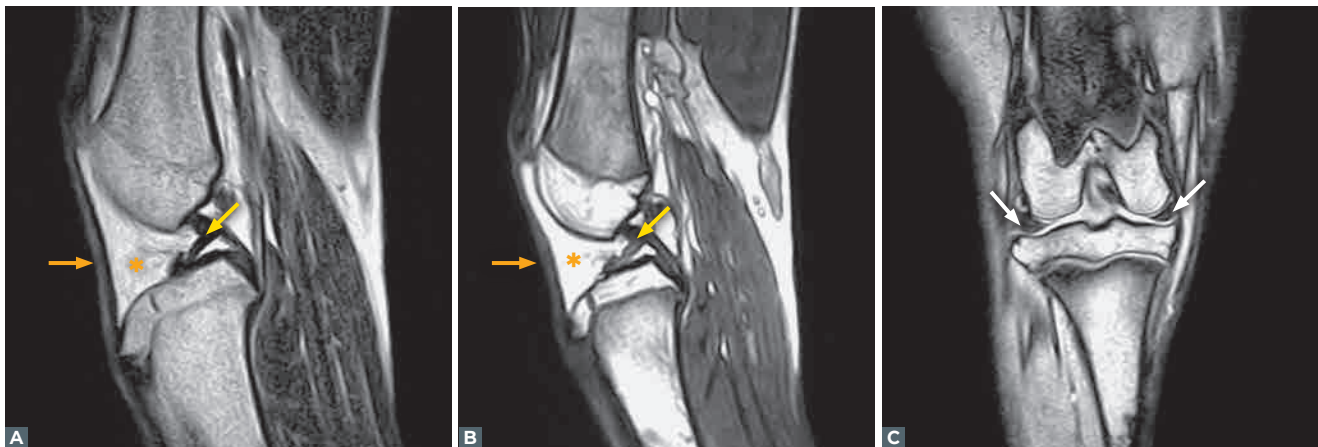 and menisci (white arrows) can be seen. The contrast between soft tissue structures is superior to that in CT images (fig. 2.8), and MRI is preferred for assessing tendons and ligaments.

The juvenile skeleton

In the fetal and juvenile dog or cat, bone develops either by endochondral or intramembranous ossification. In the case of endochondral ossification, the bone develops from mineralization and ossification of cartilage at the growth plates or physes. This is how the vertebrae and all tubular long bones in the skeleton are formed. The growth plates are interposed between the epiphysis and metaphysis, which is the site where the bone grows in length. The epiphyses are the components of the long bones which form the articular surfaces of joints. There are also separate ossification centers, termed apophyses, in many long bones at the site of origin or insertion of larger tendons and ligaments. In contrast, flat bones, such as those of the skull, scapula, or pelvis, and cuboidal bones, such as those of the carpus and tarsus, are formed by intramembranous ossification in which mineralization occurs within a fibrous connective tissue precursor of the bone without formation of cartilage. The pelvis and skull are formed by the fusion of several flat bones originating from discrete ossification centers. Incomplete ossification and fusion of multiple osseous components can make the assessment of these structures in neonatal and juvenile patients quite challenging. Apophyses are also present in some of the flat bones, such as the supraglenoid tubercle of the scapula, which is the origin of the biceps brachii muscle.

In neonatal patients, the diaphyses of long bones are partly mineralized and visible on radiographs, but the epiphyses of many long bones, cuboidal bones, apophyses, and sesamoid bones are comprised entirely of soft tissue and thus not visible on radiographs. The earliest sign of mineralization is the appearance of a small ovoid region of mineralization roughly in the center of the soft tissue precursor of the bone. Incompletely mineralized structures usually have a ragged, poorly defined margin that should not be mistaken for pathology. Complete mineralization of these ossification centers is usually present by 4 months of age. The physes or growth plates appear as a radiolucent band interposed between the epiphysis and metaphysis and are comprised of cartilage. Ossification of the cartilage occurs at the metaphyseal aspect and results in longitudinal growth of the bone. The bone is relatively wider at the metaphysis than in the diaphysis, and as the bone grows in length, osteoclastic activity at the outer cortical margin reduces the diameter. The effect of this osteoclastic remodeling is to make the outer cortical margin of the metaphysis unsharp or indistinct, and this is referred to as the cut back zone. The growth plates of the long bones close at varying times, and all are closed at maturity. Growth plate closure in normal dogs depends upon the overall body

size and growth plate location, i.e., skeletal maturity occurs at 5-6 months of age in small breeds and about 11-13 months in giant breeds (**table 2.1**). The long bone growth plates close between 5 and 13 months of age. The apophyses of the iliac crests often remain open up to 5 years of age in normal dogs. After growth plate closure, a radio-opaque band may persist at the site, sometimes referred to as a physeal scar. Closure of the long bone growth plates in normal cats may be delayed by neutering before or at the time of puberty, and open long bone growth plates may be seen in normal patients up to 2-3 years of age. For skeletally immature patients, it is often helpful to obtain radiographs of the contralateral limb to determine if the appearance represents normal variation or pathology. Similarly, if there is suspicion of systemic disease affecting the skeleton or developmental skeletal disease such as dwarfism, radiographs of a normal sibling or an age-matched individual of the same breed may be very helpful for the characterization of lesions.

Sesamoid bones are bones formed within tendons to ensure free movement of the tendon where it passes over an angular osseous structure. The largest sesamoid bone in the body is the patella, located in the tendon of insertion of the quadriceps femoris muscle. There are also large sesamoid bones in the tendons of origin of the gastrocnemius muscles, positioned at the caudal proximal aspect of the femoral condyles. Paired sesamoid bones are present at the distal aspect of the interosseous muscle in the distal metacarpus and metatarsus. There are also small, round sesamoid bones at the dorsal aspect of the metacarpophalangeal and metatarsophalangeal joints, which should not be

Table 2.1 Age at the appearance and fusion or closure of the ossification center/physes of the main bones of the appendicular skeleton			
Structure	**Location**	**Age at the appearance of the ossification center**	**Age at fusion or closure**
Radius	Proximal epiphysis/growth plate	1-2 weeks	10-13 months
	Distal epiphysis/growth plate	2-3 weeks	6-8 months
	Proximal epiphysis/growth plate	3-5 weeks	6-11 months
	Distal epiphysis/growth plate	2-4 weeks	8-12 months
Ulna	Distal epiphysis/growth plate	8 weeks	8-12 months
Pelvis	Pubis	Birth	4-6 months
	Ilium	Birth	4-6 months
	Ischium	Birth	4-6 months
	Os acetabulum	7 weeks	5 months
	Symphysis pubis		Up to 5 years
	Iliac crest	4 months	1-5 years
Femur	Proximal epiphysis (head)/growth plate	2 weeks	7-11 months
	Distal epiphysis/growth plate	2-3 weeks	8-11 months
Tibia	Proximal epiphysis/growth plate	3 weeks	6-12 months
	Distal epiphysis/growth plate	3 weeks	8-11 months
	Tuberosity	8 weeks	6-8 months to epiphysis
Fibula	Proximal epiphysis/growth plate	9 weeks	8-12 months
	Distal epiphysis/growth plate	2-7 weeks	7-11 months

mistaken for chip fractures. There is an inconsistent sesamoid bone in the tendon of origin of the ulnaris lateralis muscle at the lateral aspect of the elbow joint in larger dogs.

The adult skeleton

In skeletally mature cats and dogs, the cortices of the long bones show uniform mineralization with marked contrast to the soft tissues. The subchondral bone adjacent to the articular surface is usually more opaque, as this is a component of the bone that bears a substantial load. The margin of the subchondral bone at the joint space should be smooth and well-defined. For most joints, the contour of the articular surface of the subchondral bone will mirror that of the subchondral bone of the facing bone of the joint. In most synovial joints with normal congruency, the subchondral bone of the articular surfaces conforms to and matches each other. For example, the glenoid of the scapula has a concave margin that matches the convex contour of the humeral head. An exception to this is the normal stifle joint, where cartilaginous menisci are interposed between the condyles of the distal femur and condyles of the tibial plateau. The visibility of the joint space is dependent upon the X-ray beam being centered at the joint space and oriented parallel to the joint space, and there may be an artifactual narrowing of the joint space when the X-ray beam is centered away from the joint or the joint positioned obliquely. Joint spaces may appear quite wide in juvenile patients from incomplete ossification of the epiphyses and cuboidal bones. Joint space widening should be assessed with caution in small animals, as radiographs are rarely acquired with the patient bearing weight, and traction on the limb to ensure diagnostic positioning may result in some widening of the joint space. The trabecular bone within the epiphysis and metaphysis should have a well-defined fine honeycomb appearance, blending with the cortices. The cortices of the diaphyses of the long bones have uniform dense radiopacity. The thickness of the cortices will vary depending upon the load placed on the bone and the diameter. For example, the cortices of the humerus are slightly thinner in the proximal diaphysis than in the distal diaphysis. For most long bones, fine trabecular bone is visible within the bone at the metaphyses, while the medullary cavity in the diaphysis is usually devoid of detail. The blood supply to long bones is delivered via the nutrient artery. This passes through the cortex of the diaphysis, appearing as an oblique line usually more visible on one projection.

References

1. Thrall DE, Robertson, ID (editors). Atlas of normal radiographic anatomy and anatomic variance in the dog and cat. St Louis, Elsevier, 2011.

2. Ticer JW (editor). Radiographic techniques in small animals. Philadelphia, WB Saunders, 1975.

Appendicular skeleton: radiology and techniques

Nathalie Rademacher

KEY POINTS

❚ Sedation or anesthesia should be used for optimal image quality, particularly the positioning of appendicular skeletal radiographs.

❚ Collimation to the joint or long bones of the area of interest is recommended to eliminate distortion and minimize scatter radiation.

❚ Two orthogonal views are the minimum examination for any region of the appendicular skeleton.

❚ Additional specific projections can be acquired depending on the suspected disease process.

❚ Advanced imaging such as ultrasound, MRI, or CT may be needed especially for soft tissues, and since normal radiographs do not out completely exclude pathology.

Radiographs are the primary imaging tool for the assessment of the appendicular skeleton in cats and dogs. However, it is important to note that normal radiographs do not rule out all disease processes. Indications for radiographic examination for any region of the appendicular skeleton include, but are not limited to:

❚ Trauma.
❚ Congenital defects.
❚ Developmental diseases.
❚ Metabolic diseases.
❚ Inflammatory diseases.
❚ Infectious diseases.
❚ Neoplastic diseases.

Radiographic views should be performed in sedated or anesthetized dogs and cats to avoid motion unsharpness (**fig. 3.1**) and for radiation protection by reducing exposure of the personnel since manual restraint can be avoided, thus reducing the number of retakes (**fig. 3.2**). Furthermore, correct positioning is more easily and consistently obtained when radiographs are acquired with sedation or anesthesia, which is critical for diagnosis.

Exposures with high kVp and low mAs techniques should be chosen as there is good inherent contrast in bone, and motion artifact is minimized by the shortest possible exposure time. The technique selected should result in good radiographic contrast which will allow assessment of both the bones and soft tissues and adequate penetration of bone to show tra-

Fig. 3.1 Dorsoventral radiograph of a cat's head and neck. Patient movement results in severe unsharpness, and the image is nondiagnostic.

Fig. 3.2 Ventrodorsal radiograph of a cat obtained to assess both front legs. The patient was not sedated, and unprotected hands and wrists are exposed to the primary beam, which is a serious violation of radiation safety rules. Compounding this error, the image is nondiagnostic.

Fig. 3.3 (**A**) Underexposed ventrodorsal radiograph of the thorax of a dog resulting in decreased contrast and with the included skeletal structures appearing homogeneously white. (**B**) Lateral radiographs of the lumbar spine with moderate to severe overexposure including soft tissues, lung parenchyma, and retroperitoneal space. Planking artifact is also present.

becular detail.[1] Both under- and overexposure should be avoided: underexposure will present bones as homogeneous white structures with no visible internal detail (**fig. 3.3A**), while overexposure will reduce the visibility of the soft tissue structures (**fig. 3.3B**).

Two orthogonal views (mediolateral and craniocaudal/caudocranial or dorsopalmar/dorsoplantar) are the minimum requirement for the evaluation of any region of the appendicular skeleton.[1, 2] Several radiographs of the limb should be made, centered, and collimated to a specific region of interest in the limb rather than trying to image the entire limb in a single image, which will cause distortion and hinder diagnosis. Radiographs of the joints should include approximately one-third of the long bones proximal and distal to the joint (**fig. 3.4**). Radiographs of the long bones should include the proximal and distal joints (**fig. 3.5**). Additional radiographic views may be needed to demonstrate some abnormalities. These include:[1]

▮ Comparison radiographs.
▮ Oblique radiographs.
▮ Tangential or skyline radiographs.

❚ Stressed or compressed radiographs including traction or torsion/rotation radiographs.
❚ Weight-bearing radiographs.
❚ Serial (over time) radiographs.

Radiographs of the contralateral limb are especially helpful in immature patients to diagnose subtle abnormalities of the growth plates and epiphyses by comparison to the normal limb (**fig. 3.6**). However, it must be kept in mind that many developmental and systemic diseases will result in symmetrical changes, and radiographs of a normal sibling may be more helpful for comparison. In mature animals, comparison radiographs are usually not indicated unless needed to differentiate normal anatomic variation from pathology or to confirm a subtle or equivocal lesion (**fig. 3.7**).

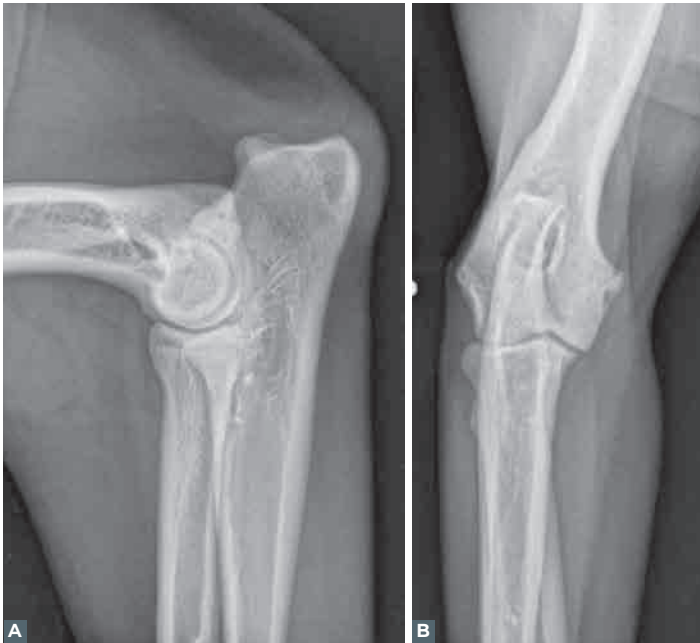Oblique radiographs project different aspects of a joint or region and maximize the

Fig. 3.4 Orthogonal mediolateral (**A**) and craniocaudal (**B**) radiographs of a normal canine left elbow to show how centering at the joint shows the joint space more clearly without distortion.

Fig. 3.5 Orthogonal mediolateral (**A**) and craniocaudal (**B**) radiographs of the right crus of a dog for surgical planning to represent an example of radiography of long bones centered and collimated to include the proximal and distal joints.
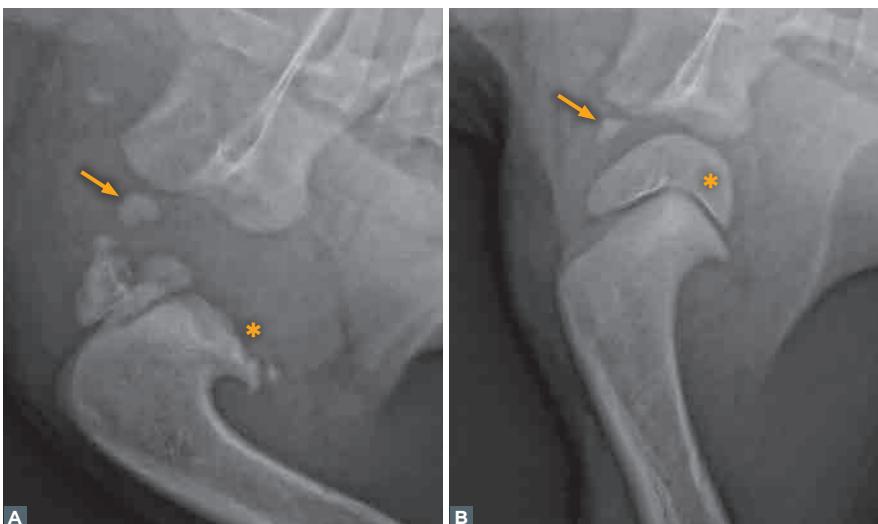
Fig. 3.6 Mediolateral radiographs of the abnormal right shoulder and normal left shoulder in a three-month-old dog with chronic right forelimb lameness. There is partial nonuniform mineralization of the most cranial aspect of the proximal epiphysis, which comprises several irregularly shaped fragments while there is no visible mineralization of the caudal two-thirds (asterisk). The proximal metaphysis has an undulating irregular contour. The apophysis of the supraglenoid tubercle is displaced caudally and distally and has less distinct margins than in the normal limb (arrows). The changes are unilateral which excludes systemic disease or an abnormality of endochondral ossification and are most likely secondary to traumatic injury as a neonate. *Arrows*, supraglenoid tubercle; *star*, humeral head epiphysis.

Fig. 3.7 Mediolateral and craniocaudal radiographs of the left antebrachium and extremity (**A-B**) of a nine-month-old spayed female Fox Terrier with chronic left forelimb lameness due to premature closure of the left distal ulnar physis resulting in a shortening of the ulna and secondary cranial bowing of the radius and valgus deviation of the carpus and foot. (**C-D**) Comparison radiographs of the normal right limb.

Fig. 3.8 (**A**, **D**) A complete set of views of the tarsus of a one-year-old spayed female Dane mix with suspicion of having been hit by a car and lameness located to the tarsus comprising (**A**) mediolateral, (**B**) dorsoplantar, (**C**) dorsomedio-450 plantarolateral oblique (DMPLO) and (**D**) dorsolateral-450 plantaromedial oblique (DLPMO) views. A moderate amount of soft tissue swelling surrounds the right tarsus. At the most proximal aspect of this swelling at the plantaromedial aspect there is an irregularly shaped, smoothly marginated cutaneous defect. Thin linear to pinpoint, well-defined mineral fragments are present in the soft tissue at the medial aspect of the talocrural joint in the region of the medial collateral ligament, at the proximal aspect of the medial malleolus of the tibia, and just distal to the medial malleolus. The soft tissue swelling is consistent with contusion and edema and the defect with a laceration. The small mineral fragments could represent avulsed bone or road debris in a wound or on the skin. Medial and lateral instability of the right talocrural joint with suspect medial collateral ligament avulsion or injury (partial or complete tear) was diagnosed by physical examination. (**E**) A flexed dorsoplantar radiograph of the left tarsus of a young dog to highlight the trochlear ridges (arrows) of the talus without superimposition of the calcaneus, used in cases of suspected osteochondritis dissecans of the talus, particularly the lateral trochlear ridge. For this projection, the dog is positioned in dorsal recumbency with the metatarsus and digits pointed to the ceiling and the beam centered at the talocrural joint space. The image is normal.

chances of projecting an edge lesion tangentially, especially in a complex joint (**fig. 3.8**).[3] The entrance point of the primary X-ray beam is typically moved 30 to 45 degrees medial (**fig. 3.8C**) or 30 to 45 degrees lateral (**fig. 3.8D**) to the entrance point used for a craniocaudal (dorsopalmar, dorsoplantar) view. Specific projections may be used to reduce superimposition when assessing complex joints, such as a flexed dorsoplantar projection of the tarsus which shows the trochlear rides of the talus without superimposition of the calcaneus (**fig. 3.8E**). Tangential or skyline radiographs (**fig. 3.8E**) (e.g., cranioproximo-craniodistal radiographs) are lesion-oriented views usually used for imaging the anatomy such as the bicipital groove of the humerus or the patellar groove of the femur and patella, e.g., in cases of sagittal patellar fractures (**fig. 3.9**).

Stress radiographs are defined as radiographs obtained with the application of a controlled force upon a joint to show and assess the severity of instability, subluxation, or luxation not apparent on standard projections (**fig. 3.10**).[4] Stress radiographs require general anesthesia to eliminate pain and ensure consistent positioning. They are made by stabilizing the limb proximal and distal to the joint

Fig. 3.9 (**A**) Mediolateral and (**B**) caudocranial radiographs of the left stifle and (**C**) a cranioproximal-craniodistal skyline view of the left distal femur and patella in a seven-year-old neutered male Doberman with acute left hind lameness after playing outside. There is intra-articular effusion in the left femorotibial joint, causing cranial displacement of the infrapatellar fat pad. There are several small, well-defined osseous fragments located at the base of the patella and within the femorotibial joint space. A complete, sagittal fracture of the left patella with sharp fracture margins can be seen superimposed on the distal femur on the caudocranial radiograph (arrows). The fracture fragments are displaced medially and laterally, exacerbated by flexion on skyline projection.

Fig. 3.10 Dorsoplantar radiographs of the left tarsus and foot with lateral (**A**) and medial (**B**) stress applied to the foot. The patient is a four-year-old spayed female Shih Tzu with lameness after jumping off the couch and with comminuted articular fractures of the distal row of the tarsal bones and head of the second metatarsal. Stress is applied with a wooden spoon to force the foot laterally (**A**) resulting in widening of the medial aspect of the tarsometatarsal joint and lateral subluxation of the metatarsals due to rupture of medial collateral ligaments and joint capsule. Stress applied to force the foot medial (**B**) shows no instability of the tarsal joints.

Fig. 3.11 (**A**) Mediolateral and (**B**) dorsopalmar radiographs of the right carpus of a seven-year-old neutered male Mastiff with chronic lameness due to suspected osteosarcoma. There is lysis of the trabecular bone in the medullary cavity of the distal radial metaphysis and epiphysis, seen on the dorsopalmar projection. Small foci of lysis are also visible in the medial cortex of the distal radius. There is periosteal new bone with nonuniform mineralization and smooth well-defined margins on the cranial, medial, and caudal cortices of the distal radial metaphysis and adjacent diaphysis. The lesion has an indistinct but relatively short transition to normal bone. Based on the lesion appearance, location, and patient signalment, osteosarcoma is the most likely diagnosis. Mild broad-based soft tissue swelling is noted along the cranial and medial aspects of the distal radius. Fine-needle aspirations were non-diagnostic. Mediolateral (**C**) and dorsopalmar (**D**) recheck radiographs of the right carpus obtained two months later show more severe circumferential soft tissue swelling of the right distal antebrachium. There is progressive new bone formation which shows relatively uniform mineralization but now has irregular poorly defined margins. There is progressive moth-eaten to permeative lysis within the medullary cavity. The lesion was confirmed as osteosarcoma by repeat fine-needle aspiration and cytology.

and applying force typically with wooden or plastic spoons to demonstrate joint laxity. Comparison stress radiographs with the normal side can be obtained if it is not certain that the extent of joint movement is pathological.[1] Compression or distraction radiographs are mainly used to confirm laxity of the coxofemoral joints for early diagnosis of hip dysplasia, such as PennHip® radiographs.[5] Serial radiographic examinations are also very useful in the investigation of orthopedic disease to assess the progression of remodeling over time, evaluate treatment response, and detect lesions not evident on initial images (**fig. 3.11**).[1,2] They are mostly used in the evaluation of fracture healing.

References

1. Muhlbauer MC, Kneller SK. Radiography of the Dog and Cat: Guide to Making and Interpreting Radiographs. New York, Wiley-Blackwell, 2013.
2. Baines E. Clinically significant developmental radiological changes in the skeletally immature dog: 1. Long bones. *In Practice* 28:188-199, 2006.
3. Thrall DE. Principles of Radiographic Interpretation of the Appendicular Skeleton. In Thrall DE (editor). Textbook of Veterinary Diagnostic Radiology 7th edition. St. Louis, Elsevier, 2018, pp 334-347.
4. Farrow C. Stress radiography: applications in small animal practice. *J Am Vet Med Assoc* 181:777-784, 1982.
5. Reagan JK. Canine Hip Dysplasia Screening Within the United States: Pennsylvania Hip Improvement Program and Orthopedic Foundation for Animals Hip/Elbow Database. *Vet Clin North Am Small Anim Pract* 47:795-805, 2017.
6. Kim SE, Lewis DD, Pozzi A. Effect of tibial plateau leveling osteotomy on femorotibial subluxation: in vivo analysis during standing. *Vet Surg* 41:465-470, 2012.

Fundamental bone and joint alterations

Nathalie Rademacher

KEY POINTS

❚ Degenerative joint disease (DJD) is the most common diagnosed orthopedic disorder.

❚ Radiographic DJD changes are non-specific and do not correlate with pain and clinical severity of lameness.

❚ Radiographically, primary bone neoplasms, metastatic neoplastic bone lesions, and osteomyelitis result in an aggressive bone lesion.

❚ In endemic areas, oligostotic bone lesions might be associated with fungal osteomyelitis.

❚ Histopathology is required for a definitive diagnosis.

❚ Benign neoplasms are uncommon.

Degenerative joint disease

Degenerative joint disease (DJD) or osteoarthrosis (OA) is the most commonly diagnosed joint disease in veterinary medicine and is a slowly progressive, irreversible degenerative disease of synovial joints characterized by pain, disability, cartilage destruction, synovitis, and bone remodeling.[1] Older dogs are usually affected; however, it is estimated that 20% of dogs one year of age or older are affected.[2] The weight-bearing joints of medium-sized to large dogs are most often affected, although it can involve any synovial joint in any dog and cat. The most frequent locations are the coxofemoral (**fig. 4.1A**), shoulder, and stifle joints. Underlying causes are numerous and include normal force on an abnormal joint (e.g., OCD, elbow [**figs. 4.1B** and **4.1B**] or hip dysplasia) or abnormal forces on a normal joint (e.g., trauma, joint instability, epiphyseal aseptic necrosis).[2]

Fig. 4.1 (**A**) Extended ventrodorsal radiographs of the pelvis of a seven-year-old, neutered male German Shepherd dog with bilateral subluxation of the coxofemoral joints with severe osteoarthrosis and severe muscle atrophy secondary to bilateral hip dysplasia. Mediolateral (**B**) and craniocaudal (**C**) radiographs of the right elbow of an eight-year-old neutered male English Bulldog with lameness associated with multiple legs. Severe degenerative changes are noted due to severe elbow osteoarthrosis, present in both elbows in this patient.

Radiographic signs develop later than the structural changes associated with DJD, and clinical signs do not correlate well with radiographic signs. Additionally, most radiographic signs of joint disease are nonspecific. Also, patients with progressive joint disease may have different signs when examined during different phases of the disease. Sound knowledge of joint pathophysiologic characteristics is as important in the diagnosis of joint disease as the ability to make and interpret radiographs of joints. Radiographic signs of DJD[3] include:

▌ Joint swelling.
▌ Decreased subchondral bone opacity.
▌ Increased subchondral bone opacity.
▌ Subchondral osseous cyst-like lesions.
▌ Perichondral bony proliferation (osteophytes).
▌ Enthesophytes.
▌ Mineralization of periarticular soft tissues.
▌ Intra-articular calcified bodies.
▌ Joint luxation, subluxation, or incongruency.
▌ Joint malformation.

Osteophytes consist of cartilage and later become radiographically visible when they become ossified. They are seen as bony outgrowths at the periphery of the articular cartilage. Enthesophytes are bony proliferations at the level of the joint capsule, ligaments, tendons, or fascia insertion into the bone.

General radiographic principles for evaluation of aggressive bone lesions

Radiographic abnormalities of bones and joints are usually divided into non-aggressive (trauma, degenerative changes) and aggressive lesions (neoplasia, osteomyelitis) based on radiographic findings. Various disease processes can have overlapping radiographic findings, and cytology or histopathology is almost always needed for a definitive diagnosis. Radiographic aggressive bone lesions result either from neoplastic or infectious causes and radiographic signs are listed here:[4]

▌ Soft tissue swelling can be either articular, periarticular, or superficial.
▌ Number of bones involved can be monostotic, oligostotic, or polyostotic.
▌ Location of the lesion might be metaphyseal, diaphyseal, or centered on a joint.
▌ Periosteal new bone formation can be the result of neoplasia, infection, trauma, or septic arthritis and can elevate the periosteum and form various patterns of periosteal reaction.
▌ Considerable overlap with different disease processes and different periosteal reactions has been reported.[5] Smooth periosteal reaction is primarily seen with benign, slow processes such as a healing fracture[5] and is a uniformly opaque single layer of new bone formation (**fig. 4.2A**). Lamellar periosteal reactions are multiple layers of bone concentrically layered like an onion skin appearance (**fig. 4.2B**). Spiculated periosteal reaction is the result of a rapid underlying process preventing the formation of new bone under the raised periosteum and is often subdivided into a columnar or palisading periosteal reaction that is radiographically seen as vertically oriented columns of new bone oriented perpendicular to the cortex (**fig. 4.2C**), whereas in sunburst periosteal reaction it radiates in a divergent pattern (**fig. 4.2 D**), and amorphous being irregular and disorganized (**fig. 4.2E**).[5]
▌ Lysis is differentiated into geographic, moth-eaten, or permeative lysis, indicating the progressive degree of aggressiveness. Geographic lysis is radiographically seen as a single, large, relatively well-defined region of bone loss (**fig. 4.3A**), whereas moth-eaten lysis is represented as multiple medium to small foci of bone loss (**fig. 4.3B**), and permeative lysis is seen as multiple pinpoint foci of bone loss (**fig. 4.3C**).[6]

Fig. 4.2 (**A**) A smooth, uniformly opaque single layer of new bone formation is noted along the tibial diaphysis in this five-year-old spayed female Siberian Husky with hypertrophic osteopathy due to a mediastinal histiocytic sarcoma. (**B**) Note the faint multiple concentric layers of bone in this male neutered seven-year-old Mastiff with lamellar periosteal reaction at the right cranio-distal radius due to osteosarcoma. (**C**) Note the vertically oriented columns of new bone oriented perpendicular to the patella cortex representing spiculated periosteal reaction of the left stifle in this seven-year-old male Mastiff diagnosed with histiocytic sarcoma. (**D**) Note the divergent pattern representing sunburst periosteal new bone formation medial along the proximal tibia in this Rottweiler with confirmed implant-associated osteosarcoma. (**E**) Note the highly disorganized and irregular new bone formation in this four-year-old spayed female Rottweiler consistent with amorphous periosteal reaction due to osteosarcoma.

Fig. 4.3 (**A**) Geographic lytic lesion seen as a well-defined, slightly irregularly marginated radiolucency noted in the right proximal femur on the mediolateral radiograph of a three-year-old male Labrador Retriever with confirmed osteosarcoma. (**B**) Craniocaudal radiograph of the right carpus in an adult spayed female Domestic medium hair cat with confirmed histo-plasmosis. Note the moth-eaten lysis of the distal ulna and radius seen as multiple small to medium-sized areas of bone loss. (**C**) Multiple faint pinpoint foci of bone loss representing permeative lysis are noted in the right humerus of an eight-year-old intact male Irish Setter with confirmed osteosarcoma at this location.

▌ A long zone of transition is characterized by an incomplete or poorly defined demarcation of the lesion to normal bone within the medullary cavity.

Bone neoplasia

Osteosarcoma is the most common primary malignant bone tumor in dogs and cats and represents more than 80% in dogs and 70% in cats of primary neoplasms originating from the skeleton,[7] followed by chondrosarcomas, fibrosarcoma, and hemangiosarcoma. Large and giant breed dogs (mainly German Shepherds, Rottweilers, Doberman Pinschers, Irish Setters and Boxers, Saint Bernards, Great Danes, Golden, and Labrador Retrievers)[7,8] are overrepresented with a bimodal age distribution (with peak incidence at 1-2 years and 7-9 years of age)[9] and in cats older than ten years. Osteosarcoma can occur anywhere in the skeleton but most commonly in the metaphyses of the distal radius (**fig. 4.4**), proximal humerus (**fig. 4.5**), distal femur and proximal and distal tibia in dogs.[9] The distal radius is associated with a lower rate of metastasis, while localization at the proximal humerus, distal femur, or proximal tibia has a high metastasis rate and increased mortality.[10] In cats, the hindlimbs seem to be more affected, and the lesion appears to be more lytic. Unlike dogs, osteosarcomas in cats are locally invasive but slow to metastasize, with an overall incidence of metastatic rate less than 10%. Appendicular osteosarcomas may be primarily lytic, primarily productive, or most commonly mixed, with lytic and productive features. Primary bone tumors typically affect a single metaphysis of a long bone and may extend into the epiphysis or diaphysis or adjacent bone joints. The occurrence of implant-associated osteosarcoma is extremely low (0.0008%).[11] Benign bone tumors such as osteoma, osteochondroma, and bone cysts are uncommon.[7]

Metastatic bone tumors arise more commonly from carcinomas than sarcomas,[12] and mammary and pulmonary neoplasms are a common source of bone metastasis[13] and can be found either in axial or appendicular skeleton (**fig. 4.6**).

Fig. 4.4 (**A**) Mediolateral and (**B**) craniocaudal radiographs of the right distal radius of an eight-year-old intact male Irish Setter. Severe soft swelling, cortical destruction, permeative lysis, and irregular periosteal new bone formation of the distal metaphysis of the right radius are present with a pathologic fracture of the distal radius and ulna with craniomedial displacement. This dog was diagnosed with osteosarcoma.

Fig. 4.5 Mediolateral radiograph of the right humerus of a nine-year-old spayed female Rottweiler with moth-eaten lysis, cortical thinning, and palisading new bone formation of the proximal metaphysis of the right humerus due to confirmed osteosarcoma.

Fig. 4.6 (**A**) Mediolateral and (**B**) craniocaudal radiograph of the right radius and ulna of a 14-year-old male Shih Tzu with confirmed metastatic carcinoma. Note the irregular, partially palisading periosteal reaction with minimal cortical destruction with a long zone of transition along the ulnar diaphysis.

Radiographic appearance can vary from bone lysis to new bone formation changes, and all the intermediates between these two extremes include soft tissue swelling, cortical destruction, periosteal reaction, a long zone of transition characterized by an incomplete or poorly defined demarcation of the lesion to normal bone within the medullary cavity and lysis of the cortex and or medulla.[4, 7] Neoplasia (primary bone tumors, metastasis) and fungal or bacterial osteomyelitis both result in radiographic aggressive bone lesions and require biopsy and histopathology for a definitive diagnosis. Additional findings such as the number of bones involved (monostotic, oligostotic, polyostotic), location (metaphyseal, diaphyseal), signalment, history, physical and laboratory findings as well as geographic location can help prioritize (**table 4.1**) for differential diagnoses. Pathologic fractures can occur without abnormal or overt trauma due to weakening of the bone (**fig. 4.4**). Radiographs remain the main imaging modality in veterinary medicine for bone neoplasia evaluation; however, CT and MRI are more and more used in veterinary medicine.[7] CT allows evaluation of bone destruction and sclerosis anatomically, which is particularly useful for axial sites. MRI can assess the tumor extent and its relationship with the surrounding structures, which is particularly interesting for axial sites, given the proximity of the vertebral canal.

Subungual tumors versus subungual infections

The digit is also a location where radiographic differentiation between infectious and neoplastic bone lesions is impossible. The most common canine subungual tumor is squamous cell carcinoma (**fig. 4.7**), commonly occurring in large breed dogs with black hair coats, followed by melanomas.[14] Inflammatory conditions of the digit are also common. Digital tumors typically involve a single digit. A syndrome of metastasis of pulmonary tumors to multiple digits has been identified in cats[15] (so-called "lung digit syndrome") (**fig. 4.8**).

Table 4.1 Summary of radiographic features for differentiation of aggressive bone lesions.			
Bone pathology	**Location**	**Mono-or polyostotic**	**Age**
Primary bone tumor	Metaphysis	Monostotic	Bimodal
Metastatic	Metaphysis or diaphysis	Polyostotic	Old
Multifocal tumors	Anywhere	Polyostotic	Old
Fungal osteomyelitis	Diaphysis	Mono-, oligostotic	Young to middle age
Bacterial osteomyelitis, hematogenous	Metaphysis	Polyostotic	Young
Bacterial osteomyelitis, penetrating trauma	Anywhere	Monostotic or adjacent bones	Any

Fig. 4.7 Dorsopalmar radiograph of the right front foot of a 16-year-old neutered male Rottweiler with a confirmed subungual melanoma affecting the fourth digit with absent P3 and aggressive bone lesion of the distal portion of P2 of the same digit with associated severe soft tissue swelling.

Fig. 4.8 (**A**) Mediolateral radiograph of the left hind foot and (**B**) plantarodorsal view of the right hind foot of a nine-year-old spayed female cat with a two-month history of swollen and ulcerated digits on the right front and bilateral hind feet. Polyostotic aggressive bone lesions affecting P3 of all digits of the left hind and third digit on the right hindlimb are noted in this cat, consistent with metastatic carcinoma. (**C**) Ventrodorsal thoracic view of the same cat as figs. 4.8A and 4.8B. A well-defined, smooth to irregularly marginated cavitary mass within the left caudal lung lobe at the level of the left caudal lobar bronchus is present. This is consistent with primary lung neoplasia, and bronchial carcinoma is confirmed.

Osteomyelitis

Osteomyelitis, the inflammation of bone and bone marrow, might be either of exogenous or hematogenous origin and might be caused by bacterial or fungal organisms, with both resulting in radiographic aggressive bone lesions.[16] Bacterial infections typically result from exogenous causes such as a penetrating injury from an open fracture and after a car accident (78%), a bite wound (17%), ascending infection due to pododermatitis (5%), or surgery (**fig. 4.9**) and, less commonly, from hematogenous spread.[17, 18] One study reported that exogenous osteomyelitis is more frequently caused by a single microorganism in 59% of cases with a predominance of Gram-positive bacteria, most frequently *Staphylococcus* spp., followed by *Streptococcus* spp., *Escherichia coli*, other enteric bacteria, and anaerobic bacteria.[16] Most lesions from bacterial osteomyelitis will have a periosteal reaction that is less aggressive than with a neoplastic lesion. Periosteal reactions with osteomyelitis often have a palisading or columnar appearance, but columnar periosteal reactions can sometimes

Fig. 4.9 (**A**) Mediolateral and (**B**) craniocaudal radiographs of the left radius and ulna of a ten-year-old neutered male Weimaraner that was bitten 10 days before and ran into a wheelbarrow after. Note the large focal soft tissue swelling of the distal ulna with amorphous periosteal reaction and focal cortical destruction due to the reported bite wound. This was confirmed as bacterial osteomyelitis.

Fig. 4.10 (**A**) Left lateral and (**B**) ventrodorsal views of the thorax of a seven-month-old intact male Pitbull with polyostotic aggressive bone lesions of the left humerus, left scapula, right ulna, and multiple ribs with miliary nodular pulmonary pattern and sternal lymphadenopathy confirmed due to coccidioidomycosis.

be found with neoplastic bone lesions as well. Hematogenous bacterial osteomyelitis lesions are usually polyostotic and occur in young dogs and therefore are not typical for neoplastic disease. Sampling and microbiologic testing should always be performed before the initiation of any treatment.

Fungal osteomyelitis should be considered when polyostotic aggressive bone lesions are present. Typically, large breed young adults are affected, generally of hematogenous origin, and are most commonly identified in geographic endemic areas, such as the Midwest/Mississippi valley and Eastern USA and Canada (blastomycosis) and the desert southwest (coccidioidomycosis) regions of the United States (**fig. 4.10**). However, cases may be seen in non-endemic regions when infected dogs are relocated or become infected when traveling, and a complete travel history should be obtained. Dogs with osteomyelitis caused by *Coccidioides* spp. were younger and weighed less compared to dogs with osteosarcoma in a recently published study with axial lesions and nonadjacent polyostotic disease more common, but the radiographic appearance did not differ between osteomyelitis and osteosarcoma.[19] Fungal osteomyelitis in cats is rare, with the most commonly reported being histoplasmosis[20] (**fig. 4.11**) with a high prevalence in the Midwest and

Fig. 4.11 (**A**) Mediolateral radiograph of the right radius and ulna and (**B**) craniocaudal radiograph of the right carpus in a female spayed Domestic medium hair cat of unknown age with confirmed fungal osteomyelitis due to histoplasmosis affecting the distal radius and ulna as well as the proximal ulna.

South of the US, with inflammatory arthritis a common presentation.[20] However, over the past 20 years, the incidence of opportunistic fungal infection has increased substantially in dogs receiving multiagent immunosuppressive therapy, with a recent study showing an incidence of 6.5% in dogs being treated for immune-mediated disease.[21]

References

1. McLaughlin R. Management of chronic osteoarthritic pain. *Vet Clin North Am Small Anim Pract* 30:933-949, ix, 2000.

2. Johnston SA. Osteoarthritis. *Vet Clin North Am Small Anim Pract* 27:699-723, 1997.

3. Allan G, Davies S. Radiographic signs of joint disease in dogs and cats. In Thrall DE (editor). Textbook of Veterinary Diagnostic Radiology 7th edition. St. Louis, Elsevier, 2016, pp 403-433.

4. Thrall DE. Principles of radiographic interpretation of the appendicular skeleton. In Thrall DE (editor). Textbook of Veterinary Diagnostic Radiology 7th edition. St. Louis, Elsevier, 2016, pp 334-347.

5. Rana RS, Wu JS, Eisenberg RL. Periosteal reaction. *AJR Am J Roentgenol* 193:W259-272, 2009.

6. Thrall DE. Radiographic features of bone tumors and bone infections in dogs and cats. In Thrall DE (editor). Textbook of Veterinary Diagnostic Radiology 7th edition. St. Louis, Elsevier, 2016, pp 390-402.

7. Vanel M, Blond L, Vanel D. Imaging of primary bone tumors in veterinary medicine: which differences? *Eur J Radiol* 82:2129-2139, 2013.

8. Szewczyk M, Lechowski R, Zabielska K. What do we know about canine osteosarcoma treatment? Review. *Vet Res Commun* 39:61-67, 2015.

9. Guim TN, Bianchi MV, De Lorenzo C, Gouvea AS, Gerardi DG, Driemeier D, et al. Relationship between clinicopathological features and prognosis in appendicular osteosarcoma in dogs. *J Comp Pathol* 180:91-99, 2020.

10. Schmidt AF, Nielen M, Klungel OH, Hoes AW, de Boer A, Groenwold RH, et al. Prognostic factors of early metastasis and mortality in dogs with appendicular osteosarcoma after receiving surgery: an individual patient data meta-analysis. *Prev Vet Med* 112:414-422, 2013.

11. Arthur EG, Arthur GL, Keeler MR, Bryan JN. Risk of osteosarcoma in dogs after open fracture fixation. *Vet Surg* 45:30-35, 2016.

12. Cooley DM, Waters DJ. Skeletal metastasis as the initial clinical manifestation of metastatic carcinoma in 19 dogs. *J Vet Intern Med* 12:288-293, 1998.

13. Trost ME, Inkelmann MA, Galiza GJ, Silva TM, Kommers GD. Occurrence of tumours metastatic to bones and multicentric tumours with skeletal involvement in dogs. *J Comp Pathol* 150:8-17, 2014.

14. Grassinger JM, Floren A, Muller T, Cerezo-Echevarria A, Beitzinger C, Conrad D, et al. Digital lesions in dogs: A statistical breed analysis of 2912 cases. *Vet Sci* 8:136, 2021.

15. Gottfried SD, Popovitch CA, Goldschmidt MH, Schelling C. Metastatic digital carcinoma in the cat: a retrospective study of 36 cats (1992-1998). *J Am Anim Hosp Assoc* 36:501-509, 2000.

16. Siqueira EG, Rahal SC, Ribeiro MG, Paes AC, Listoni FP, Vassalo FG. Exogenous bacterial osteomyelitis in 52 dogs: a retrospective study of etiology and in vitro antimicrobial susceptibility profile (2000-2013). *Vet Q* 34:201-204, 2014.

17. Gieling F, Peters S, Erichsen C, Richards RG, Zeiter S, Moriarty TF. Bacterial osteomyelitis in veterinary orthopaedics: pathophysiology, clinical presentation and advances in treatment across multiple species. *Vet J* 250:44-54, 2019.

18. Rabillard M, Souchu L, Niebauer GW, Gauthier O. Haematogenous osteomyelitis: clinical presentation and outcome in three dogs. *Vet Comp Orthop Traumatol* 24:146-150, 2011.

19. Shaver SL, Foy DS, Carter TD. Clinical features, treatment, and outcome of dogs with Coccidioides osteomyelitis. *J Am Vet Med Assoc* 260:63-70, 2021.

20. Fielder SE, Meinkoth JH, Rizzi TE, Hanzlicek AS, Hallman RM. Feline histoplasmosis presenting with bone and joint involvement: clinical and diagnostic findings in 25 cats. *J Feline Med Surg* 21:887-892, 2019.

21. Dedeaux A, Grooters A, Wakamatsu-Utsuki N, Taboada J. Opportunistic fungal infections in small animals. *J Am Anim Hosp Assoc* 54:327-337, 2018.